01 Nov 2003

Study of the Electronic Properties of Some Ytterbium Filled Skutterudites by Magnetic Susceptibility and X-ray Absorption and Tin-119 Mössbauer Spectroscopy

Fernande Grandjean
Missouri University of Science and Technology, grandjeanf@mst.edu

Gary J. Long
Missouri University of Science and Technology, glong@mst.edu

Bernard M. Mahieu

Ji Hui Yang

et. al. For a complete list of authors, see https://scholarsmine.mst.edu/chem_facwork/825

Recommended Citation

F. Grandjean et al., "Study of the Electronic Properties of Some Ytterbium Filled Skutterudites by Magnetic Susceptibility and X-ray Absorption and Tin-119 Mössbauer Spectroscopy," *Journal of Applied Physics*, vol. 94, no. 10, pp. 6683-6691, American Institute of Physics (AIP), Nov 2003.
The definitive version is available at https://doi.org/10.1063/1.1623609

Study of the electronic properties of some ytterbium filled skutterudites by magnetic susceptibility and x-ray absorption and tin-119 Mössbauer spectroscopy

Fernande Grandjean
Department of Physics, B5, University of Liège, B-4000 Sart-Tilman, Belgium

Gary J. Long[a)]
Department of Chemistry, University of Missouri-Rolla, Rolla, Missouri 65409-010

Bernard Mahieu
Department of Chemistry, CSTR, Université Catholique de Louvain, Place L. Pasteur, 1, B-1348 Louvain-la-Neuve, Belgium

J. Yang and G. P. Meisner
General Motors Research and Development Center, Warren, Michigan 48090

D. T. Morelli
Delphi Automotive Systems Research Laboratory, Cherry Creek Corporate Park, 51786 Shelby Parkway, Shelby Township, Michigan 48315

(Received 14 July 2003; accepted 15 September 2003)

Magnetic susceptibility, ytterbium L_{III}-edge x-ray absorption and tin-119 Mössbauer spectral measurements have been carried out to probe the electronic structure of ytterbium and tin in the filled or partially filled skutterudite compounds, $Yb_yCo_4Sb_{12-x}Sn_x$, over a range of x and y values. The ytterbium valence obtained from the magnetic susceptibility and ytterbium L_{III}-edge x-ray absorption measurements is in excellent agreement and clearly reveals an evolution from intermediate valence ytterbium for $x=0$ to nearly divalent ytterbium for $x=0.8$. This evolution parallels an increase in the unit cell volume and hence in the ytterbium site volume available as the tin content increases. The tin-119 Mössbauer spectral hyperfine parameters indicate, without question, that tin substitutes on the antimony sublattice of the skutterudite structure. Further, the tin electronic configuration is both very similar to that of the antimony in the structure and insensitive to the ytterbium content, y. © *2003 American Institute of Physics.* [DOI: 10.1063/1.1623609]

I. INTRODUCTION

Filled skutterudite compounds have been extensively studied over the past few years because of their promise as highly efficient thermoelectric converters.[1] One of the attractive features of these compounds is the very low lattice thermal conductivity that arises when a rare-earth atom occupies, or ''fills,'' a void in the skutterudite crystal lattice.[2] Although the reduction in the thermal conductivity is predominantly a lattice dynamical effect, the filling rare-earth atom also contributes electrons to the conduction band of the parent skutterudite compound and, thus, also alters its electronic properties. Although most rare-earth atoms in intermetallic compounds are trivalent, there are notable exceptions, including the well known tendency of cerium to assume both the $4f^0$ and $4f^1$ electronic configurations, i.e., both the respective trivalent and tetravalent configurations in cerium filled skutterudites.

Recently, the synthesis of the ytterbium filled skutterudite, $YbFe_4Sb_{12}$, and the partially filled $Yb_yCo_4Sn_xSb_{12-x}$ skutterudite compounds has been reported.[3] The latter compounds were made in an attempt to partially compensate for the ''extra'' electrons added by the ytterbium with holes arising from the substitution of tin for antimony.[4,5] Generally speaking, as is the case for cerium, the ytterbium in intermetallic compounds tends to exhibit ambivalent electronic characteristics with a propensity, depending on the chemical environment, for exhibiting either the divalent $4f^{14}$ or the trivalent $4f^{13}$ electronic configuration, or an intermediate valence electronic configuration. Clearly, in order to better understand, predict, and control the technologically important thermoelectric properties of filled skutterudite compounds, it is necessary to obtain a good description of their electronic structure, particularly of the electronic configuration of ytterbium in $YbFe_4Sb_{12}$ and $Yb_yCo_4Sn_xSb_{12-x}$.

A very clear indication of the ytterbium valence or electronic configuration in $YbFe_4Sb_{12}$ and in the partially filled $Yb_yCo_4Sn_xSb_{12-x}$ compounds is their magnetic susceptibility. Because the parent $CoSb_3$ compound, the unfilled skutterudite, is a diamagnetic semiconductor, any magnetic moment arising from the insertion of ytterbium into the $CoSb_3$ lattice can be very easily measured. The distinction between the divalent closed f-shell, $4f^{14}$ configuration, which has no magnetic moment, and the trivalent $4f^{13}$ configuration, which has a single f-shell hole and hence a magnetic moment, is straightforward.

[a)]Author to whom correspondence should be addressed; electronic mail: glong@umr.edu

Another very powerful technique for determining the ytterbium valence in these compounds is x-ray absorption near-edge structure spectroscopy, XANES spectroscopy. In this method a high-energy photon is absorbed by an inner core electron of an atom, exciting the latter to the first available unoccupied state. The energy at which the transition occurs is related to the ground state electronic configuration of the atom. Recently, the ytterbium L_{III}-edge XANES spectra of $YbFe_4Sb_{12}$ at room temperature have been reported[6,7] and the results indicate an effective ytterbium valence of 2.16 and 2.68. In addition, the ytterbium L_{III}-edge XANES spectra of $Ce_xYb_yFe_4Sb_{12}$ indicate[7] that ytterbium has a non-integral valence dependent upon *y*.

In order to more clearly understand the charge state of ytterbium in skutterudites, and its evolution with compositional changes and with temperature, we have undertaken a magnetic susceptibility and an L_{III}-edge XANES study of the $Yb_yCo_4Sb_{12-x}Sn_x$ series of compounds. Further, in order to obtain a deeper understanding of the electronic structure of these compounds by probing a second crystallographic site in the structure, we have carried out a tin-119 Mössbauer spectral study.

II. EXPERIMENTAL TECHNIQUES

The samples studied herein are identical to those previously prepared and studied.[8] For magnetic susceptibility measurements, a few hundred milligrams of material were placed in a polyethylene capsule which was inserted inside a polyethylene straw and lowered into a Quantum Design magnetometer. After establishing that the magnetization was a linear function of field, measurements were carried out from 2 to 300 K in a field of 0.5 T. The empty capsule/straw combination was measured in order to determine their magnetization, for which the results were corrected.

The ytterbium L_{III}-edge XANES spectra were obtained at 295 K on beam line 4-3 at the Stanford Synchrotron Radiation Laboratory, Stanford, California. The measurements were carried out in transmission mode with a Si(111) $\phi=90°$ double-crystal monochromator using ion chambers filled with a mixture of nitrogen and helium and placed both in front and behind the sample. The low-temperature ytterbium L_{III}-edge XANES spectra were obtained between 10 and 200 K on beam line 7-3 at the Stanford Synchrotron Radiation Laboratory. In order to improve the signal to noise ratio, the low temperature measurements were carried out in fluorescence mode with a Si(111) $\phi=90°$ double-crystal monochromator and a Lyttle detector with a filter of nickel. Harmonic contamination was minimized by detuning the monochromator. The spectra were recorded between 8795 and 8925 eV with a step of 10 eV and between 8925 and 8980 eV with a step of 0.35 eV. The *K*-edge absorption spectrum of a thin copper foil was used for energy calibration.

The tin-119 Mössbauer spectra of $Yb_{0.19}Co_4Sb_{11.9}Sn_{0.1}$, $Yb_{0.19}Co_4Sb_{11.5}Sn_{0.5}$, and $Yb_{0.5}Co_4Sb_{12-x}Sn_x$, with $x=0.5$, 0.6, 0.7, and 0.8, were measured at 83 K and the spectra of $Yb_{0.5}Co_4Sb_{11.2}Sn_{0.8}$ were measured between 83 and 340 K on a constant-acceleration spectrometer which was calibrated with α-iron foil. The tin-119 spectra were obtained with a room temperature tin-119*m* source in a $CaSnO_3$ matrix and the isomer shifts are reported relative to $CaSnO_3$. The absorber thicknesses were $\sim$65 mg/cm^2 and the samples were dispersed in boron nitride powder. The spectra were fit with a symmetric quadrupole doublet and the resulting isomer shifts, quadrupole splittings, and linewidths are accurate to $\sim\pm0.02$ mm/s.

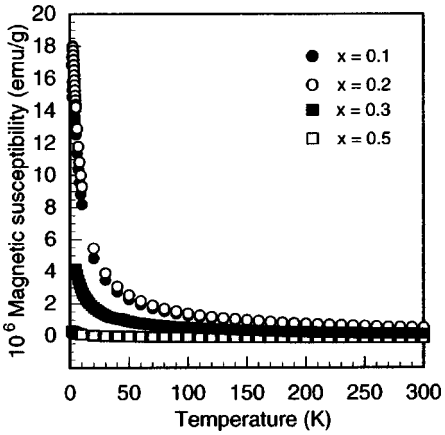

FIG. 1. Magnetic susceptibility of the $Yb_{0.19}Co_4Sb_{12-x}Sn_x$ compounds as a function of temperature.

III. MAGNETIC MEASUREMENTS

The temperature dependence of the magnetic susceptibility of $Yb_yCo_4Sb_{12-x}Sn_x$, with $y=0.19$ and 0.5, is shown in Figs. 1 and 2, respectively. A sample of the unfilled $CoSb_3$ skutterudite was found to be diamagnetic with a susceptibility similar to that reported previously.[9,10] Upon ytterbium filling, a paramagnetic moment develops as is shown in Figs. 1 and 2. As is indicated in Fig. 3 for $Yb_{0.19}Co_4Sb_{11.5}Sn_{0.5}$ and in Fig. 4 for $Yb_{0.5}Co_4Sb_{11.5}Sn_{0.5}$, the molar susceptibility can be obtained from the Curie law

$$\chi=\chi_0+\frac{C}{T}, \tag{1}$$

where χ_0 is the diamagnetic contribution to the susceptibility and *C* is the Curie constant. The high temperature slope of a

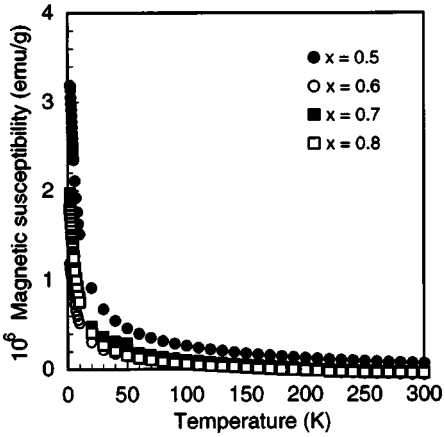

FIG. 2. Magnetic susceptibility of the $Yb_{0.5}Co_4Sb_{12-x}Sn_x$ compounds as a function of temperature.

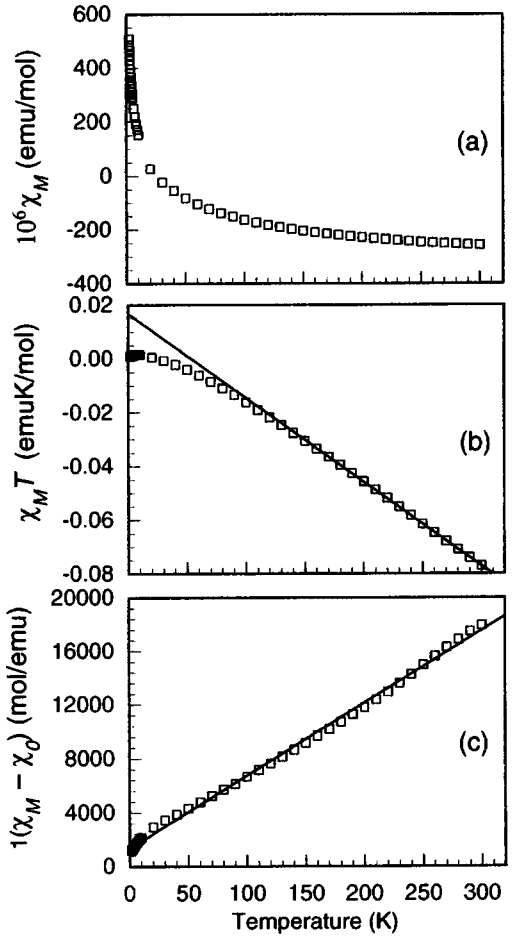

FIG. 3. The temperature dependence of the observed molar magnetic susceptibility, χ_M, (a), $\chi_M T$, (b), and $1/(\chi_M - \chi_0)$, (c), obtained for $Yb_{0.19}Co_4Sb_{11.5}Sn_{0.5}$. The slope of the high temperature $\chi_M T$ values shown in (b) yields the diamagnetic susceptibility, χ_0. The slope of $1/(\chi_M - \chi_0)$ shown in (c) yields the Curie constant.

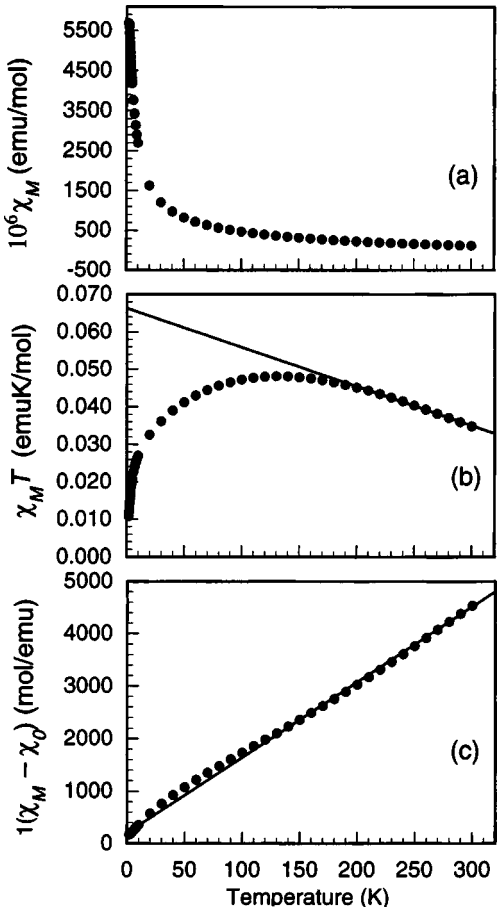

FIG. 4. The temperature dependence of the observed molar magnetic susceptibility, χ_M, (a), $\chi_M T$, (b), and $1/(\chi_M - \chi_0)$, (c), obtained for $Yb_{0.5}Co_4Sb_{11.5}Sn_{0.5}$. The slope of the high temperature $\chi_M T$ values shown in (b) yields the diamagnetic susceptibility, χ_0. The slope of $1/(\chi_M - \chi_0)$ shown in (c) yields the Curie constant.

plot of $\chi_M T$ vs T, see Figs. 3(b) and 4(b), yields the diamagnetic contribution to the susceptibility. It should be noted that in Eq. (1) the χ_0 term may also include other temperature independent contributions to the susceptibility such as any temperature independent paramagnetism and any Pauli paramagnetism, both of which are expected to be negligible in the compounds under study. By subtracting this negative diamagnetic susceptibility, see Table I, from the observed susceptibility, the slope of the resulting plot of $1/(\chi_M - \chi_0)$ versus T, see Figs. 3(c) and 4(c), yields the Curie constant. Most likely as a result of crystal field effects[11] the $1/(\chi_M - \chi_0)$ vs T plots in Figs. 3(c) and 4(c) and, for all compounds, in Figs. 5 and 6, show some curvature mostly at low temperature. Hence, the Curie constants given in Table I were obtained from the high temperature slope of these plots. From the Curie constant, the effective moment, p, of ytterbium in $CoSb_3$ was obtained from

$$p = \left[\frac{3k_B C}{yN_A\mu_B^2}\right]^{1/2}, \tag{2}$$

where k_B is the Boltzmann constant, N_A is Avogadro's number, μ_B is the Bohr magneton, y is determined by the stoichiometry of the $Yb_yCo_4Sb_{12-x}Sn_x$ compound, and C is in units of (emu K)/(mol Yb). Because divalent ytterbium has no magnetic moment, whereas trivalent ytterbium is expected to have a moment of $4.54\,\mu_B$, an effective valence for the ytterbium in $Yb_yCo_4Sb_{12-x}Sn_x$ can be obtained from

$$v_x = 2 + \frac{p}{4.54}, \tag{3}$$

where it is assumed, as expected,[10] that the antimony, tin, and low-spin cobalt are all diamagnetic. The effective ytterbium valence, see Table I, is plotted, as a function of tin content in $Yb_yCo_4Sb_{12-x}Sn_x$, as the solid symbols in Fig. 7.

IV. XANES SPECTRAL MEASUREMENTS

The 295 K ytterbium L_{III}-edge XANES spectra of $Yb_yCo_4Sb_{12-x}Sn_x$ and their fits are shown in Fig. 8. All spectra exhibit a two-peak white line which is characteristic of a mixture of two ytterbium ground state electronic configurations. The peak at ~8940 eV corresponds to the $4f^{14}$ electronic ground state configuration, or the so-called divalent ytterbium, whereas the peak at ~8950 eV corresponds to the $4f^{13}$ electronic ground state configuration, or the so-called trivalent ytterbium. All the low temperature ytterbium

TABLE I. Magnetic properties of the $Yb_yCo_4Sb_{12-x}Sn_x$ compounds.

Compound	χ_0, emu/mol Yb	C, emu K/mol Yb	p, μ_B/Yb	v_x
$Yb_{0.19}Co_4Sb_{11.9}Sn_{0.1}$	-1.29×10^{-4}	1.23	3.14	2.69
$Yb_{0.19}Co_4Sb_{11.8}Sn_{0.2}$	-2.51×10^{-4}	1.45	3.41	2.75
$Yb_{0.19}Co_4Sb_{11.7}Sn_{0.3}$	-1.30×10^{-3}	0.68	2.34	2.51
$Yb_{0.19}Co_4Sb_{11.5}Sn_{0.5}$	-1.65×10^{-3}	0.088	0.85	2.19
$Yb_{0.5}Co_4Sb_{11.5}Sn_{0.5}$	-2.19×10^{-4}	0.17	1.18	2.26
$Yb_{0.5}Co_4Sb_{11.4}Sn_{0.6}$	-5.80×10^{-4}	0.135	1.04	2.22
$Yb_{0.5}Co_4Sb_{11.3}Sn_{0.7}$	-4.38×10^{-4}	0.101	0.90	2.20
$Yb_{0.5}Co_4Sb_{11.2}Sn_{0.8}$	-3.41×10^{-4}	0.056	0.68	2.15

L_{III}-edge XANES spectra obtained between 4.2 and 200 K for $Yb_{0.5}Co_4Sb_{11.5}Sn_{0.5}$ and $Yb_{0.5}Co_4Sb_{11.2}Sn_{0.8}$ are identical to the room temperature spectra.

The observed two-peak white line is often interpreted in terms of a nonintegral ytterbium valence state and this approach is followed herein. After the subtraction of a linear pre-edge background and normalization, the spectra have been fit with Eq. (4)

$$\mu(E)=\frac{A_1}{A_1+A_2}\left\{0.5+\frac{1}{\pi}\arctan\left(\frac{E-(E_0)}{\Gamma_1/2}\right)\right\}+\frac{A_2}{A_1+A_2}\left\{0.5+\frac{1}{\pi}\arctan\left(\frac{E-(E_0+\delta)}{\Gamma_1/2}\right)\right\}+\frac{\left(\frac{\Gamma}{2}\right)^2 A_1}{(E-E_1)^2+(\Gamma/2)^2}+\frac{\left(\frac{\Gamma}{2}\right)^2 A_2}{(E-E_1-\delta)^2+(\Gamma/2)^2}. \quad (4)$$

In this equation, the two arctangent functions represent the continuum and the two Lorentzian functions represent the $2p_{3/2}\rightarrow5d$ transitions for the $4f^{14}$ and $4f^{13}$ electronic ground state configurations of ytterbium, the divalent and trivalent ytterbium states, respectively. E_0 is the energy of the onset of the continuum, E_1 is the energy at which the $2p_{3/2}\rightarrow5d$ transition occurs, Γ is the width of the transition, and A_1 and A_2 are the areas of the Lorentzian peak for the divalent and trivalent ytterbium, respectively. Because a shift of ~9 eV, the so-called replicate splitting, is expected between the continuum onset and the absorption peak of the two ytterbium states, the onset of the continuum and the energy of the peak for the trivalent ytterbium are shifted by the replicate splitting, δ. The arctangent function has a linewidth, Γ_1, which is determined[7] by the experimental resolution provided by the monochromator and reproduces well the steep rising edge of the white line. The linewidth, Γ, of the Lorentzian function is of the order of 3 eV, see Table II, and is characteristic[7] of the core-hole lifetime.

The fits obtained with Eq. (4) are excellent as is shown in Fig. 8; the fitted parameters at 295 K are given in Table II. Virtually identical parameters were obtained for $Yb_{0.5}Co_4Sb_{11.5}Sn_{0.5}$ and $Yb_{0.5}Co_4Sb_{11.2}Sn_{0.8}$ between 10 and 200 K.

The energies E_0 and E_1 are independent of tin content within their error limit which is taken to be one energy step, i.e., 0.35 eV. The replicate splitting, δ, increases with increasing tin content. A similar increase of the replicate splitting with ytterbium content in $Ce_xYb_yFe_4Sb_{12}$ has been observed.[7] In $Yb_{0.5}Co_4Sb_{12-x}Sn_x$ and in $Ce_xYb_yFe_4Sb_{12}$, the lattice parameter increases[4,7] with x and y, respectively. Hence, we conclude that the replicate splitting increases with the lattice parameter. A different view of this increase is given by FEFF[13,14] modeling of the XANES profile, see below. The ytterbium valence obtained from the Lorentzian areas, A_1 and A_2, is given in Table II and is also shown as

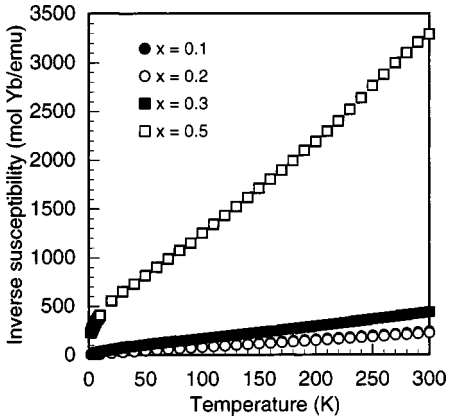

FIG. 5. Inverse magnetic susceptibility of the $Yb_{0.19}Co_4Sb_{12-x}Sn_x$ compounds after subtraction of the diamagnetic contribution to the magnetic susceptibility.

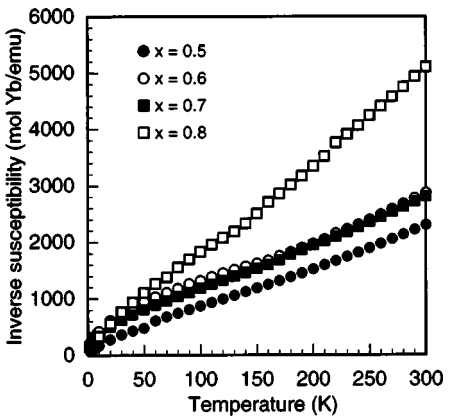

FIG. 6. Inverse magnetic susceptibility of the $Yb_{0.5}Co_4Sb_{12-x}Sn_x$ compounds after subtraction of the diamagnetic contribution to the magnetic susceptibility.

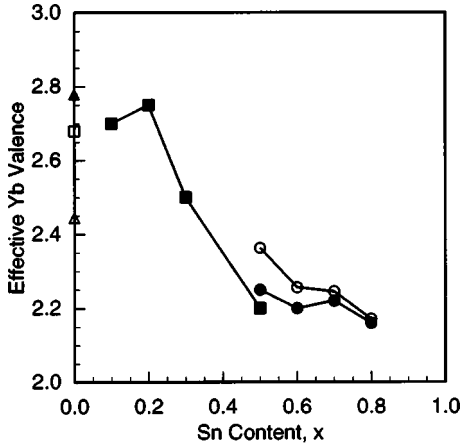

FIG. 7. The ytterbium valence in $Yb_yCo_4Sb_{12-x}Sn_x$ as a function of the tin concentration as determined by magnetic susceptibility measurements, solid symbols, and Yb L_{III}-edge XANES spectroscopy, open circles and triangle. The open square for $YbFe_4Sb_{12}$ is taken from Ref. 6.

the open circles and triangle in Fig. 7. The open squares are the previously measured[6,7] ytterbium valence in $YbFe_4Sb_{12}$.

In order to determine how the ytterbium valence is affected by the fitting model used to fit the XANES profile, we have tried different models. For instance, we have used two Lorentzian peaks to represent the two $2p_{3/2} \rightarrow 5d$ transitions, for the $4f^{14}$ and $4f^{13}$ electronic ground state configurations of ytterbium, and one arctangent function at an onset energy, E_0, which is larger than the energies of the two transitions. This fit for the $x=0$ and 0.8 samples gave ytterbium valences of 2.5 and 2.32, respectively. In order to check the sensitivity of the ytterbium valence upon the number of adjustable parameters in Eq. (4), we have carried out, for all five samples, several series of fits in which different parameters were held constant. First, E_0, E_1, and Γ_1 were constrained equal to 8936.2, 8940.8, and 1.3 eV, respectively. All these fits are satisfactory but slightly poorer than those of Fig. 8 and yield ytterbium valences which differ by only 0.01 from those given in Table II. Second, in addition to the above constraints, δ was constrained equal to 8.2 eV and all these fits were significantly poorer than those shown in Fig. 8; the resulting ytterbium valences are 0.04 larger than those given in Table II. Third, in a series of fits, E_0 and E_1 were constrained equal to 8936.2 and 8940.8 eV, respectively, and the linewidths Γ and Γ_1 were held equal. These fits are significantly poorer than those shown in Fig. 8 and yielded ytterbium valences which are 0.04 larger than those given in Table II. Finally, the fits with a model identical to that used in Ref. 7, i.e., a model in which E_0 is constrained equal to E_1 in Eq. (4), are the poorest of all the fits but the ytterbium valences differ by only 0.01 from those given in Table II. Hence, we estimate an error of $\sim \pm 0.05$ for the ytterbium valence given in Table II and we conclude that the dependence of the ytterbium valence on tin content shown in Fig. 7 is independent of the fitting model.

On the very short XANES time scale of 10^{-15} s, a mixture of divalent and trivalent ytterbium is observed at all temperatures between 10 and 295 K and results in a nonintegral, or *intermediate* valence. From a similar analysis of

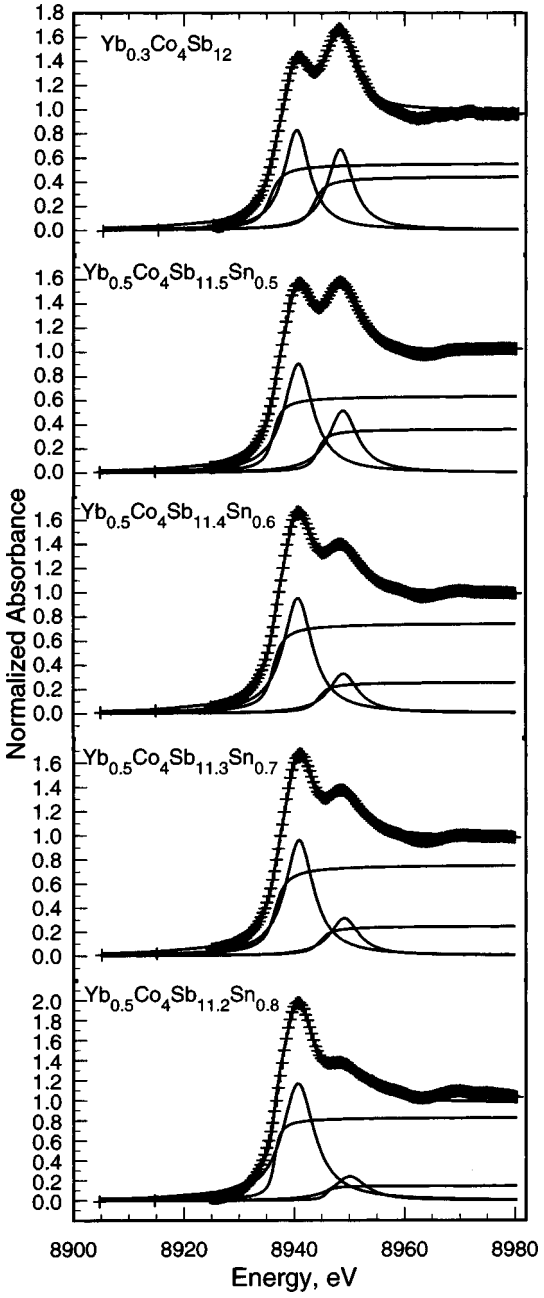

FIG. 8. The room temperature ytterbium L_{III}-edge XANES spectra with fits of $Yb_{0.3}Co_4Sb_{12}$ and $Yb_{0.5}Co_4Sb_{12-x}Sn_x$, with $x=0.5$, 0.6, 0.7, and 0.8.

the ytterbium L_{III}-edge XANES spectra of the $Ce_xYb_yFe_4Sb_{12}$ series of compounds, Bérardan *et al.*[7] concluded that the nonintegral valence of ytterbium resulted from a mixture of two different ytterbium sites with different valences, sites whose proportions change with x and y and are not differentiated by x-ray diffraction measurements. In our view, the presence of two different valence states for one ytterbium crystallographic site in these semiconducting compounds in which the $4f$ states are hybridized[12] with the iron $3d$ and antimony $5p$ states, is rather unlikely. We prefer to describe the electronic configuration of the ytterbium atom in terms of a mixture of two electronic ground states, the $4f^{14}$ and $4f^{13}$ electronic configurations, states whose proportions change with composition but not with temperature and lead

TABLE II. Ytterbium L_{III}-edge XANES E_0 and E_1 energies, replicate splitting, δ, line widths, Γ and Γ_1, in eV, and the ytterbium valence in $Yb_yCo_4Sb_{12-x}Sn_x$.

y	x	E_0	E_1	δ	Γ	Γ_1	Yb valence
0.3	0	8935.7	8940.5	7.86	2.84	1.51	2.45
0.5	0.5	8936.2	8940.8	8.06	3.19	1.20	2.36
0.5	0.6	8936.2	8940.7	8.26	3.21	1.35	2.26
0.5	0.7	8936.5	8940.9	8.20	3.13	1.49	2.25
0.5	0.8	8936.4	8940.8	9.38	3.52	0.78	2.17

to an apparent ytterbium *intermediate* valence.

Over the past few years the huge increase in computing power has made possible full multiple scattering calculations[13,14] of XANES spectra. The modeling of the XANES spectra through these calculations offers an alternative interpretation of the above results, an alternative which strongly supports the above interpretation in terms of a mixture of ground state electronic configurations. The calculations have been carried[13–15] out with FEFF8.10 for $YbCo_4Sb_{12}$. Because the first ytterbium neighbor of a given ytterbium atom is located at a large distance of 8 Å, no attempt has been made to model the partial filling of the ytterbium site in the skutterudite structure. The calculations were carried out with an 8 Å cluster centered on a central ytterbium atom. In order to take into account the two ytterbium ground state electronic configurations, self-consistent field calculations have been carried[16] out, first, for the $4f^{13}5d^1$ to L_{III} hole-$4f^{13}5d^2$ channel and, second, for the $4f^{14}5d^0$ to L_{III} hole-$4f^{14}5d^1$ channel. The calculated XANES spectra for these two channels are shown in Fig. 9. The near-edge structure of the $4f^{14}5d^0$ to L_{III} hole-$4f^{14}5d^1$ channel is found ~9 eV below the near-edge structure of the $4f^{13}5d^1$ to L_{III} hole-$4f^{13}5d^2$ channel, as is observed experimentally and, thus, the observed replicate splitting is well reproduced by the 8 Å cluster calculations. Further, some destructive and constructive interferences appear between 8970 and 9020 eV.

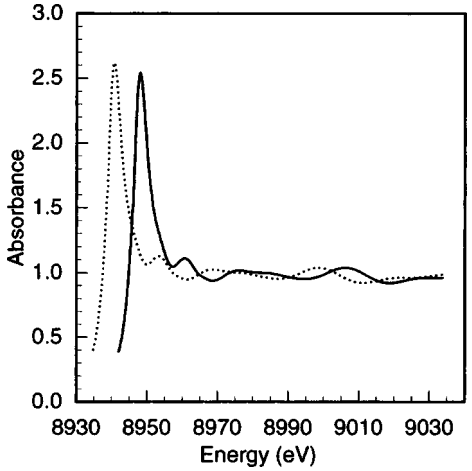

FIG. 9. The calculated (see Refs. 13–16) ytterbium L_{III}-edge XANES spectra for the $4f^{13}5d^1$ to L_{III} hole-$4f^{13}5d^2$ channel, solid line, and for the $4f^{14}5d^0$ to L_{III} hole-$4f^{14}5d^1$ channel, dotted line.

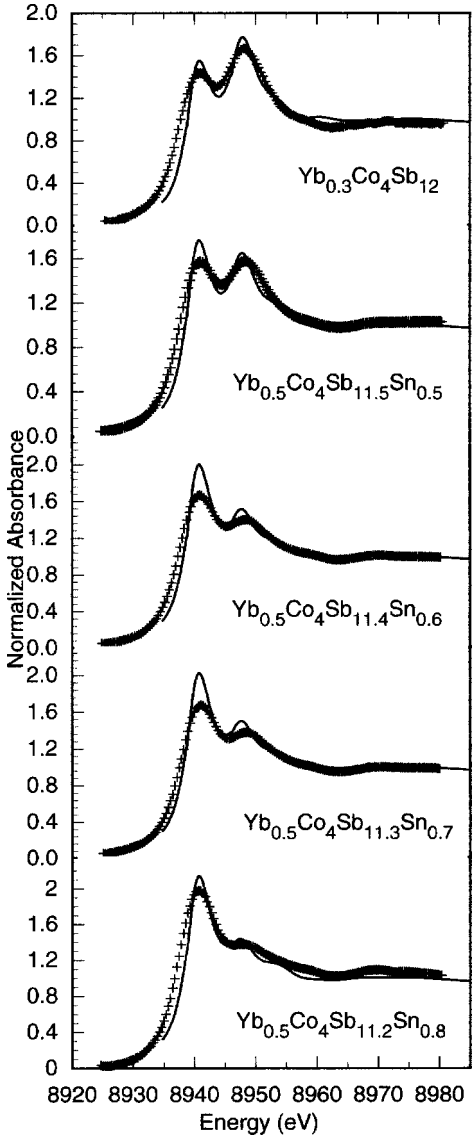

FIG. 10. The room temperature ytterbium L_{III}-edge XANES spectra of $Yb_{0.3}Co_4Sb_{12}$ and $Yb_{0.5}Co_4Sb_{12-x}Sn_x$, with $x=0.5$, 0.6, 0.7, and 0.8 with the linear combinations of the two $4f^{13}5d^1$ to L_{III} hole-$4f^{13}5d^2$ and $4f^{14}5d^0$ to L_{III} hole-$4f^{14}5d^1$ channels.

Linear combinations of the two profiles shown in Fig. 9 have been calculated and are compared with the experimental spectra in Fig. 10. The weighting coefficients of the linear combinations shown in Fig. 10 correspond to the ytterbium valence given in Table II. Because, except for these weighting coefficients, there is no free parameter involved in the calculations, the agreement between the calculated and experimental spectra is reasonably good, especially when an instrumental broadening is taken into account. Because the calculations have been carried out for the crystallographic parameters of $Yb_{0.3}Co_4Sb_{12}$, there is a slight difference between the calculated and measured energies of the peak at ~8948 eV, a difference which was observed in Table II and results no doubt from the variation of the lattice parameters with tin substitution on the antimony sublattice.

In conclusion, from the analysis of the XANES spectra both by the conventional method as given by Eq. (4) and by full multiple scattering calculations, the electronic ground

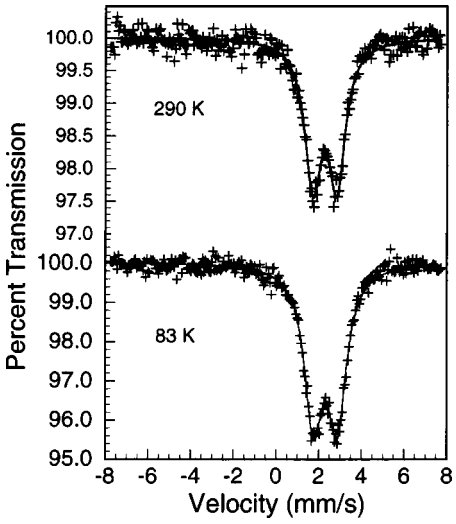

FIG. 11. The tin-199 Mössbauer spectrum of $Yb_{0.5}Co_4Sb_{11.2}Sn_{0.8}$ obtained at 83 and 290 K.

state of ytterbium is found to be a mixture of the $4f^{13}5d^1$ and $4f^{14}5d^0$ electronic configurations in the $Yb_{0.5}Co_4Sb_{12-x}Sn_x$ series of skutterudites.

V. TIN-119 MÖSSBAUER SPECTRAL MEASUREMENTS

The tin-119 Mössbauer spectra of $Yb_{0.19}Co_4Sb_{11.9}Sn_{0.1}$, $Yb_{0.19}Co_4Sb_{11.5}Sn_{0.5}$, and $Yb_{0.5}Co_4Sb_{12-x}Sn_x$, with $x=0.5$, 0.6, 0.7, and 0.8, are all very similar and typical spectra for $Yb_{0.5}Co_4Sb_{11.2}Sn_{0.8}$ are shown in Fig. 11. The corresponding hyperfine parameters for the compounds are given in Table III.

A comparison of the $Yb_{0.5}Co_4Sb_{12-x}Sn_x$ spectra with those of related tin-containing skutterudites[17] clearly indicates that the observed doublet must be assigned to tin which resides on the antimony sublattice of the basic $CoSb_3$ skutterudite structure. The observed isomer shift of ~2.3 mm/s is typical of tin in an intermetallic compound and, as expected for the open framework structure of $CoSb_3$, its isomer shift and hence *s*-electron density at the tin-119 nucleus is smaller than that observed in β tin.

TABLE III. Tin-119 Mössbauer spectral parameters.

Compound	T, K	δ, mm/s[a]	ΔE_Q, mm/s	Γ, mm/s
$Yb_{0.19}Co_4Sb_{11.9}Sn_{0.1}$	83	2.26	1.08	1.10
$Yb_{0.19}Co_4Sb_{11.5}Sn_{0.5}$	83	2.32	1.16	1.00
$Yb_{0.5}Co_4Sb_{11.5}Sn_{0.5}$	83	2.30	1.14	1.05
$Yb_{0.5}Co_4Sb_{11.4}Sn_{0.6}$	83	2.32	1.11	1.03
$Yb_{0.5}Co_4Sb_{11.3}Sn_{0.7}$	83	2.32	1.13	1.02
$Yb_{0.5}Co_4Sb_{11.2}Sn_{0.8}$	340	2.25	1.14	1.10
	290	2.27	1.12	0.95
	263	2.26	1.13	1.00
	230	2.31	1.14	1.05
	190	2.29	1.12	1.06
	180	2.29	1.13	1.04
	150	2.29	1.13	1.10
	140	2.29	1.13	1.04
	120	2.28	1.14	1.01
	83	2.31	1.11	1.04

[a]Isomer shifts are given relative to room temperature $CaSnO_3$.

The tin-119 isomer shift follows a simple function[18] of the effective number of $5s$ and $5p$ electrons given by

$$\delta = -0.38 + 3.10\ n_s - 0.20\ n_s^2 - 0.17\ n_s n_p, \tag{5}$$

where δ is the isomer shift referred to $CaSnO_3$ and n_s and n_p are the effective number of $5s$ and $5p$ electrons, respectively. Equation (5) indicates that the electronic configuration of tin in the filled skutterudites is between $5s^{0.9}5p^0$ and $5s^{1.15}5p^3$. For comparison, the antimony-121 isomer shift[19] in $CoSb_3$ is more negative than in InSb, in which antimony is $5s^15p^3$. Hence, the $5s$ electron density at the antimony nucleus is higher in $CoSb_3$ and antimony has an electronic configuration between $5s^{1+x}5p^3$ and $5s^15p^{3-x}$. Electronic band structure calculations[20] give a $5s$ population of 1.77, in good agreement with the interpretation of the antimony isomer shift. In conclusion, tin and antimony on the 24*g* site of the filled skutterudite structure have very similar electronic configurations.

Further, the low symmetry at the antimony site in the skutterudite structure leads to a substantial quadrupole splitting of ~1.15 mm/s for the tin substituted onto this site. The antimony-121 Mössbauer spectrum of unfilled skutterudite, $CoSb_3$, reported by Kjekshus, Nicholson, and Rakke yielded a quadrupole interaction of 9 mm/s and an asymmetry parameter, η, of 1.0. From this quadrupole interaction and by using a ground state nuclear quadrupole moment[21] of 0.28 barn and $R_Q=1.34$ for antimony-121, an electric field gradient at the antimony site of $3.0\times10^{22}\,V/m^2$ is obtained. From the ~1.15 mm/s quadrupole splitting measured herein and by using a nuclear quadrupole moment[22] of 0.064 barn for the tin-119*m* excited state, an electric field gradient at the tin site of $2.8\times10^{22}\,V/m^2$ is obtained. This close to perfect agreement provides excellent support for the assignment of this quadrupole doublet to tin which replaces antimony in the skutterudite structure.

The similarity of the hyperfine parameters given in Table III indicates that, as expected, the electronic properties of the rather isolated tin atoms are independent of the tin content, at least for x less than ~1.0, and do not change as the ytterbium electronic configuration changes. This is expected because there are only 0.5 ytterbium atoms per formula unit and the probability of having one ytterbium as a near neighbor of tin is quite small because the antimony 24*g* site has only one ytterbium near neighbor at a distance of ~3.4 Å.

In order to investigate the dynamic properties of the tin atom in the skutterudite lattice, the tin-119 Mössbauer spectra of $Yb_{0.5}Co_4Sb_{11.2}Sn_{0.8}$ have been measured between 83 and 353 K. The temperature dependence of the isomer shift and the logarithm of the absorption area are shown in Fig. 12 along with a linear least-square fit. The slope, $d\delta/dT$, of -2.094×10^{-4} (mm/s)/K yields[23] an effective vibrating mass of 230 g/mol for tin-119, a rather large value which seems rather anomalous. However, the correlation coefficient of the least-squares fit is poor. Hence, in order to estimate the range of values for the effective vibrating mass, the slope, $d\delta/dT$, was calculated from the isomer shifts at 83 and 340

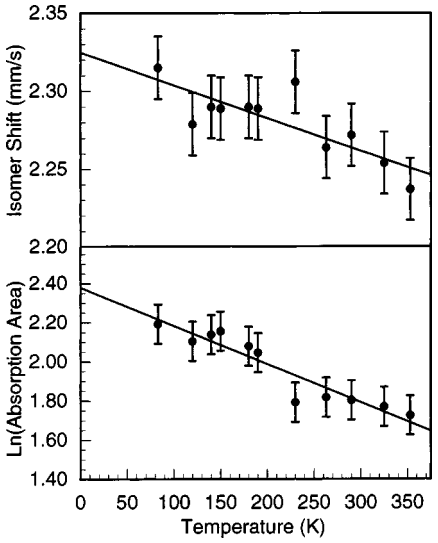

FIG. 12. The temperature dependence of the tin-119 isomer shift and natural logarithm of the Mössbauer spectral absorption area for $Yb_{0.5}Co_4Sb_{11.2}Sn_{0.8}$.

K, with their error limits of ± 0.02 mm/s. From the resulting slope of $-2.6(\pm 1.5)\times 10^{-4}$ (mm/s)/K an effective vibrating mass of 160 ± 60 g/mol is obtained. This effective vibrating mass, which is larger than the mass of 119 g/mol, indicates that the tin atom is covalently bound into the antimony sublattice of the skutterudite structure, i.e., there is strong covalency within the Sb_3Sn moiety just as there is within the Sb_3Sn moiety in the skutterudite structure. Further, the value of 160 g/mol is similar to the values observed[23] for $BaSnO_3$ and $CaSnO_3$. If the slope of the linear least-square fit in Fig. 12, $d\ell nA/dT$, of $-2.72\times 10^{-3}\,K^{-1}$ is used,[23] a Mössbauer lattice temperature, θ_M, of 256 K is obtained and if the slope of the isomer shift and logarithm of the area are used in combination, a Mössbauer lattice temperature, θ'_M, of 220 ± 40 K is obtained. These Mössbauer lattice temperatures are lower than those observed[23] for $BaSnO_3$, $CaSnO_3$, and $LiFeSnO_4$. These low values indicate that the tin atom experiences rather large atomic mean-square displacements, as was observed by Nolas *et al.*[24] However, these authors used this observation as an indication that tin fills the voids in the skutterudite structure, a filling which is ruled out by the present Mössbauer spectral results.

VI. DISCUSSION

The ytterbium valence as a function of tin concentration in $Yb_yCo_4Sb_{12-x}Sn_x$ as determined by both the XANES and magnetic susceptibility measurements, see Fig. 7, unequivocally demonstrates that the electronic ground state of ytterbium evolves from a 50–50 mixture of the $4f^{13}5d^1$ and $4f^{14}5d^0$ electronic configurations for $x=0$ to a nearly pure $4f^{14}5d^0$ electronic configuration for a tin substitution of ~ 7 at. %, i.e., for $x=0.8$. This evolution is consistent with the observation that the $CoSb_3$ lattice expands upon tin substitution,[4] an expansion that makes it more energetically favorable for the larger Yb^{2+} ion to fit into the rare-earth site. In this respect, ytterbium behaves differently than does cerium[25,26] in $Ce_xFe_{4-y}Co_ySb_{12}$, in which cerium is trivalent and does not change valence with the cobalt content.

The interpretation of all the XANES rare-earth L_{III}-edge measurements[7,25,26] on $Yb_yCo_4Sb_{12-x}Sn_x$ and $Ce_xYb_yFe_4Sb_{12}$ leads to the conclusion that, independent of composition, cerium is trivalent, whereas ytterbium adopts an *intermediate* valence which is composition dependent even when both rare-earth atoms are simultaneously present in the same lattice. This difference in valence behavior of cerium and ytterbium is rather surprising and will be further investigated through a systematic calculation of the XANES spectra with the multiple scattering approach, an approach which explores in depth the relationship between the structural and electronic properties of these materials.

The tin-119 Mössbauer spectra of the $Yb_yCo_4Sb_{12-x}Sn_x$ compounds show, without question, that tin substitutes on the antimony sublattice of the skutterudite structure. This substitution agrees with that observed[26] in $RhSb_3$ but contrasts with the tin filling of the voids previously reported[24] in $CoSb_3$. The tin-119 hyperfine parameters indicate that the tin electronic configuration is between $5s^{0.9}5p^0$ and $5s^{1.15}5p^3$; the electronic configuration is very similar to the antimony electronic configuration and is not influenced by the ytterbium content.

ACKNOWLEDGMENTS

The authors acknowledge with thanks the help of Dr. J. Y. Raty and R. P. Hermann of the University of Liège, and Dr. S. George and Dr. M. Latimer of SSRL, Stanford University. The efficient, helpful, courteous, and easily available staff at SSRL make experimental work there very pleasant. The authors also thank Professor J. J. Rehr and Dr. A. Ankudinov for their invaluable help in modifying the FEFF8.10 code to model the intermediate valence XANES spectra. G.J.L. thanks the Francqui Foundation of Belgium for his appointment as a ''Chaire Francqui Interuniversitaire au titre étranger'' during the 2002–2003 academic year.

[1] For two recent reviews, see C. Uher in *Semiconductors and Semimetals*, edited by T. M. Tritt (Academic, San Diego, 2000), Vol. 69, p. 139; G. S. Nolas, D. T. Morelli, and T. M. Tritt, Annu. Rev. Mater. Sci. **29**, 89 (1999).
[2] D. T. Morelli and G. P. Meisner, J. Appl. Phys. **77**, 3777 (1995).
[3] N. R. Dilley, E. J. Freeman, E. D. Bauer, and M. B. Maple, Phys. Rev. B **58**, 6287 (1998).
[4] N. R. Dilley, E. D. Bauer, M. B. Maple, and B. C. Sales, J. Appl. Phys. **88**, 1948 (2000).
[5] G. S. Nolas, M. Kaeser, R. T. Littleton, and T. M. Tritt, Appl. Phys. Lett. **77**, 1855 (2000).
[6] A. Leithe-Jasper, D. Kaczorowski, P. Rogl, J. Bogner, M. Reissner, W. Steiner, G. Wiesinger, and C. Godart, Solid State Commun. **109**, 395 (1999).
[7] D. Bérardan, C. Godart, E. Alleno, St. Berger, and E. Bauer, J. Alloys Compd. **351**, 18 (2003).
[8] J. Yang and G. P. Meisner, General Motors Research and Development Center Research Report No. MPL-125, 2001; J. Yang, D. T. Morelli, G. P. Meisner, W. Chen, J. S. Dyck, and C. Uher, Phys. Rev. B **67**, 165207 (2003).
[9] D. T. Morelli, T. Caillat, J.-P. Fleurial, A. Borshchevsky, J. Vandersande, B. Chen, and C. Uher, Phys. Rev. B **51**, 9622 (1995).
[10] J. Yang, G. P. Meisner, D. T. Morelli, and C. Uher, Phys. Rev. B **63**, 014410 (2001).
[11] B. D. Dunlap and G. K. Shenoy, Phys. Rev. B **12**, 2716 (1975).
[12] L. Nordström and D. J. Singh, Phys. Rev. B **53**, 1103 (1996).
[13] A. L. Ankudinov, B. Ravel, J. J. Rehr, and S. D. Conradson, Phys. Rev. B

58, 7565 (1998).
[14] J. J. Rehr and R. C. Albers, Rev. Mod. Phys. **72**, 621 (2000).
[15] Crystallographic parameters used in the calculations: $a=9.106$ Å and Sb positional parameters, $x=0$, $y=0.3368$, $z=0.1593$.
[16] In FEFF8.10 the default ytterbium ground and excited state electronic configurations are $4f^{13}5d^1$ and L_{III} hole-$4f^{14}5d^1$. Hence, to calculate the XANES spectrum for the $4f^{13}5d^1$ to L_{III} hole-$4f^{13}5d^2$ transition, a modification was introduced in subroutine getorb to put the core-hole potential screening electron in a d orbital and, for the $4f^{14}5d^0$ ground state and L_{III} hole-$4f^{14}5d^1$ transition, the default ytterbium ground state electronic configuration was modified in subroutine getorb.
[17] G. J. Long, F. Grandjean, B. Mahieu, G. Nolas, and S. Schujman (unpublished).
[18] P. A. Flinn, in *Mössbauer Isomer Shifts*, edited by G. K. Shenoy and F. E. Wagner (North-Holland, Amsterdam, 1978), p. 593.
[19] A. Kjekshus, D. G. Nicholson, and T. Rakke, Acta Chem. Scand. **27**, 1315 (1973).
[20] I. Lefebvre-Devos, M. Lasalle, X. Wallart, J. Olivier-Fourcade, L. Monconduit, and J. C. Jumas, Phys. Rev. B **63**, 125110 (2001).
[21] *Mössbauer Effect Data Index*, edited by J. G. Stevens and V. E. Stevens (Plenum, New York, 1975), p. 130.
[22] In Ref. 21, p. 136.
[23] R. H. Herber, in *Chemical Mössbauer Spectroscopy*, edited by R. H. Herber (Plenum, New York, 1981), p. 199.
[24] G. S. Nolas, H. Takizawa, T. Endo, H. Schellinschegg, and D. C. Johnson, Appl. Phys. Lett. **77**, 52 (2000).
[25] F. Grandjean, G. J. Long, R. Cortes, D. T. Morelli, and G. P. Meisner, Phys. Rev. B **62**, 12569 (2000).
[26] D. Bérardan, C. Godart, E. Alleno, E. Leroy, and P. Rogl, J. Alloys Compd. **350**, 30 (2003).